Received: 7 August 2023 | Revised: 24 September 2023 | Accepted: 15 October 2023

DOI: 10.1002/app.54850

RESEARCH ARTICLE

Applied Polymer SCIENCE WILEY

Interphase of polyoctenamer-single-wall carbon nanotubes by thermogravimetric analysis in air

Mircea Chipara[1] | Dorina Chipara[1] | Karen Martirosyan[1] | Ananta Adhikari[2] | Alexandro Trevino[1]

[1]Department of Physics and Astronomy, The University of Texas Rio Grande Valley, Edinburg, Texas, USA

[2]Department of Physics, State University of New York, Potsdam, New York, USA

Correspondence
Mircea Chipara, Department of Physics and Astronomy, The University of Texas Rio Grande Valley, 1201 University Drive, Edinburg, TX 78539, USA.
Email: mircea.chipara@utrgv.edu; chipara@yahoo.com

Funding information
NSF, Directorate for Mathematical and Physical Sciences, Grant/Award Number: 2122178

Abstract

Non-isothermal thermogravimetric analysis in air, of polyoctenamer-single wall carbon nanotubes (PO-SWNTs), loaded by various amounts of SWNTs up to 10% wt., at different heating rates (ranging from 5 to 40°C/min) is reported. The thermal degradation in the air of PO_SWNTs is dominated by a main single sigmoidal dependence, assigned to the polymer and eventually polymer-nanofiller interphase, over which a weaker sigmoid assigned to the thermo-oxidative degradation of the nanofiller is superimposed at higher temperatures. The temperature at which the nanocomposite's residual mass fraction reaches x% wt. of the initial mass, $T_{x\%}$, is reported (for $x = 5$, 50, and 85). The dependence of $T_{x\%}$ on the heating rate and the loading by nanotubes is analyzed. The temperature derivative of the thermograms defines new parameters (inflection residual mass fraction and inflection temperature) and (degradation) width. Their dependence on the loading by SWNTs was reported. Estimation of the interphase in polymer-based nanocomposites is based on the postulate that the dependence of the inflection temperature on the composition of the nanocomposite obeys a Fox-like dependence, where the bulk polymer and the polymer trapped within the interphase are considered as a blend of two miscible polymers. Complementary Raman, x-ray diffraction, and differential scanning calorimetry support these results.

KEYWORDS

differential scanning calorimetry, Fox–Flory equation, polyoctenamer-single wall carbon nanotubes interphase, Raman and wide-angle x-ray scattering, thermogravimetric analysis, thermo-oxidative degradation and inflection temperature, weight fraction of the interphase

1 | INTRODUCTION

Polymer-based nanocomposites are obtained by dispersing various types of nanoparticles within polymeric matrices. Due to the flexibility of the polymeric matrix, the macromolecular chains may wrap around the nanoparticles. This configuration is frequently stabilized by various interactions between the nanofiller and the polymeric matrix. Conformation and configuration-related interactions occur via geometrical (steric), molecular mechanical processes (interlocking, entanglements,[1,2] and collisions between the polymeric segments and the nanofiller). Neutral interactions between atoms or groups of atoms (Van der Waals and Lennard Jones potentials[3]) and electrical mediated interactions (Casimir,[4] dipole–dipole, dipole-induced dipole[5–7]) have been also reported. The extreme

case is usually represented by hydrogen bonds,[8] or even covalent bonds between (groups) of atoms belonging to the nanofiller and the polymeric matrix, respectively. These interactions trigger changes in the physical properties of the polymeric matrix in the close vicinity of the nanofiller.

The boundary between the nanofiller and the polymeric matrix is recognized as a polymer-nanofiller interface that theoretically has no thickness. Consequently, the interface is just an imaginary surface separating the nanofiller from the matrix, with no thickness and accordingly with zero volume and by consequence no mass.

In real materials, the transition between the nanofiller and the matrix extends over a few (finite number of) atoms, thus adding to the interface a certain non-zero thickness. This kind of "real interface" is recognized as the "interphase", where the separation between the nanofiller and the matrix extends over a few atoms (and hence has a finite and non-zero thickness) characterized by a certain non-zero volume. As this volume contains atoms (in most cases from both matrix and filler), the interphase is characterized by a non-zero mass, named interphase mass. By contrast, the interface has (by definition) zero thickness and consequently no volume and no mass.

Thus, the thermodynamic discrimination between interphase and interface becomes clear: interphase-related features should be controlled by the extensive thermodynamic features of the material while the interface properties should be reflected solely by intensive thermodynamic features. It was recognized that in bulk samples the standard extensive quantity is the mass while the temperature is a standard (classic) extensive thermodynamic parameter (as reflected by melting, crystallization, or glass transition temperature at the limit of large masses). This is not completely accurate; in the cases where the interphase has a thickness within the nanometer range, transition temperatures may become size-dependent. This implies that confinement effects are no longer negligible, causing a dependence of the above-mentioned transition temperatures on mass. Consequently, standard intensive quantities may include extensive features, most of them reflecting the confinement at such a small scale.[9–13] It was reported elsewhere[14,15] that submicron confinement shifts the glass transition temperature (for example in thin films) without a necessary change in the mass of the film. The polymers confined within such "nano-interphases" exhibit modified physical properties compared to the bulk polymeric matrix showing modifications of the glass,[16] melting,[17] crystallization[18] temperatures, modified mechanical properties,[19–21] and altered thermal stability.[22] Such confinement issues also affect the nanofiller. However, this manuscript will focus on the polymeric components and hence the submicron confinement effects on nanofillers will not be considered, analyzed, or discussed.

The manuscript demonstrates the capabilities of thermogravimetric analysis (TGA) in the sensing, characterization, and quantization of the interphase. It is recognized that the standard analysis of TGA data may provide solely qualitative support for the presence of the interphase. An original approach is suggested to achieve the estimation of the thickness of the interphase for cylinder-like nanoparticles (single-walled carbon nanotubes [SWNTs]) dispersed within a polymeric matrix (polyoctenamer [PO]).

2 | MATERIALS AND EXPERIMENTAL METHODS

The raw materials, SWNTs (90% purity) with an average length of about 15 microns, average external diameter ranging from 1 to 2 nm, and an average internal diameter ranging between 0.8 and 1.6 nm, were purchased from Cheaptubes Inc. Polyoctenamer was gratefully provided (as Vestenamer 8012) by Struktol Company of America. PO has an average degree of crystallinity of about 30%, a glass transition temperature of −65°C, and a melting temperature of 55°C. Both SWNTs and PO were used as received.

PO-SWNTs nanocomposites have been obtained by melt mixing at 50°C, using a counter-rotating two-screw mixer (POLYLAB) with various concentrations of SWNTs (0, 0.05, 0.10, 0.25, 0.50, 1.00, 2.50, 5.00, 7.50, and 10% wt. SWNTs).

The thermal stability of PO-SWNTs has been investigated by TGA using a TA Instruments Q50 spectrometer. The measurements have been performed in air at various heating rates (5, 10, 20, 30, and 40°C/min).

Complementary data were obtained by wide angle x-ray scattering (WAXS), using a Bruker Discovery 8 spectrometer, Raman spectroscopy, using a Renishaw InVia confocal microscope operating at 785 nm, and differential scanning calorimetry (DSC) by Using a Q 100 DSC (TA Instruments), operating in a nitrogen atmosphere.

3 | EXPERIMENTAL RESULTS

3.1 | Standard critical analysis of thermograms

The temperature dependence of the residual mass on temperature is referred to as a thermogram. Figure 1a–d

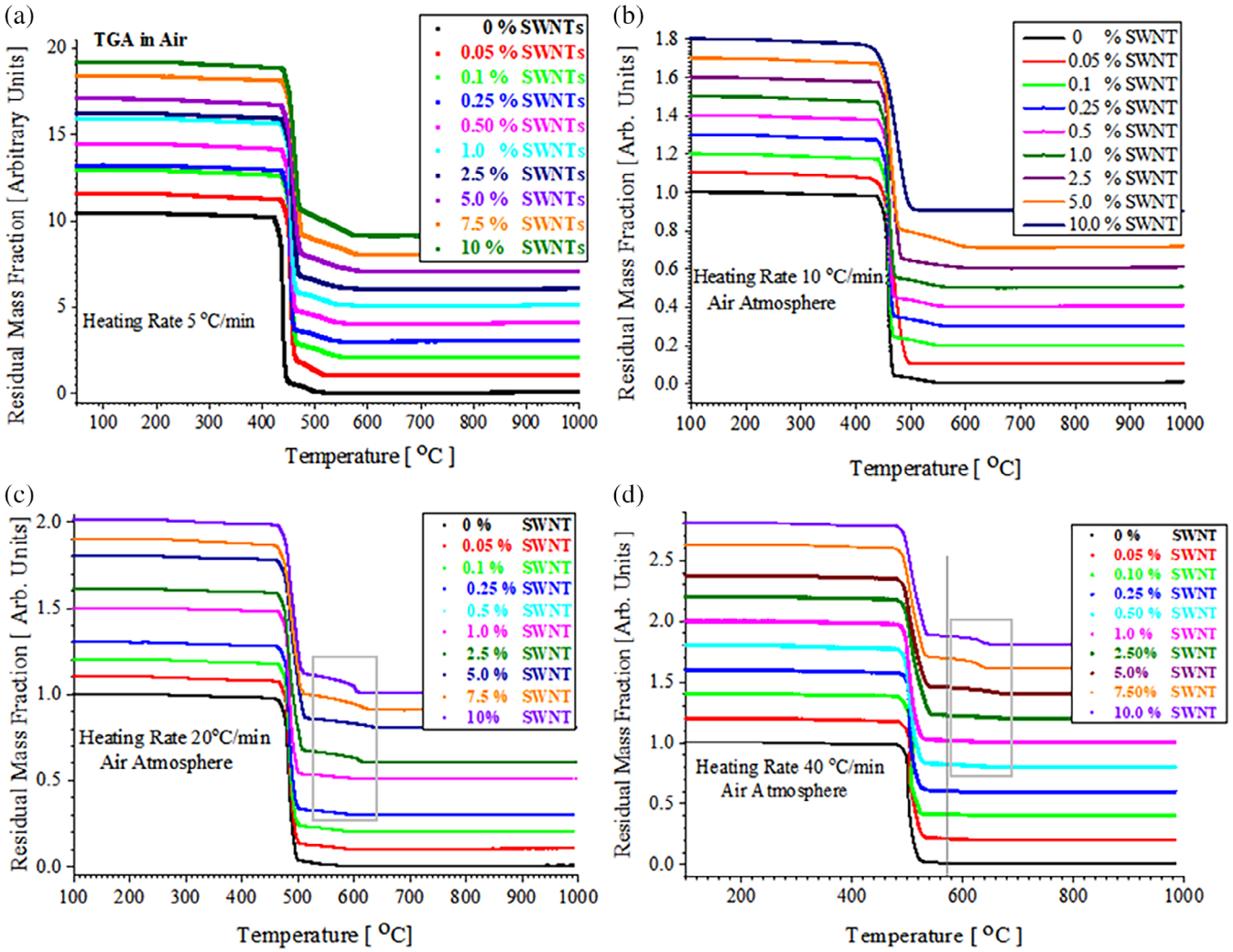

FIGURE 1 (a–d) Thermograms of polyoctenamer-single wall carbon nanotubes (PO-SWNTs) nanocomposites loaded by various amounts of SWNTs (in wt%) at different heating rates, in air. [Color figure can be viewed at wileyonlinelibrary.com]

collect the recorded thermograms for various PO-SWNTs, performed in an oxygen-containing atmosphere (air). The actual thermograms represent the residual mass fraction as a function of temperature. All thermograms were normalized; however, the thermograms shown in Figure 1a–d have been shifted upwards by the same amount, for a better visualization. Samples with various loadings by SWNTs, ranging between 0 and 10% wt. were measured. Data obtained at various heating rates (5, 10, 20, and 40°C/min) were obtained. A brief analysis of Figure 1a–d concludes that the thermal degradation of PO-SWNTs nanocomposites in air, at different loading by nanofiller, and various heating rates, is dominated by single sigmoidal-like dependencies, for loading by SWNT smaller or equal to 0.05% (wt.) and slow heating rates (below 20°C/min). These sigmoids were assigned to the thermal oxidation of the polymeric matrix and were recognized as the dominant contribution in all samples. These dominant thermograms, reflecting the main thermal degradation process(es) occurring in the samples, were shifted to higher temperatures as the heating rates were increased, in both pristine PO and PO–SWNTs nanocomposites.

At larger concentrations of SWNTs and higher heating rates, another weak sigmoid is noticed within the temperature range of 550°C up to about 650°C, depending on the heating rate and SWNTs concentration. These (weaker) sigmoids were shifted towards higher temperatures as the heating rate was increased. This additional component may reflect competing thermo-oxidative degradation of the interphase, of the SWNTs, of volatile products, or a combination of these processes. Because these high-temperature (weak and additional) components were not noticed in the thermograms of the pristine polymer at any heating rate, it was concluded that they originate from the thermal oxidation of SWNTs in

the air. This assignment is in excellent agreement with TGA data reported elsewhere[23–25] that demonstrated that the inflection temperature (i.e., the temperature at which the mass loss rate is maximum) for the thermal degradation in the air of SWNTs is ranging between 525 and 545°C[24] and respectively at about 600°C.[25] A very small amount of residue (about 0.2%) was reported for HiPCo SWNTs degraded in the air above 800°C.[23] The inflection temperatures for carbon nanotubes thermally degraded in the air were reported from 550 to 750°C.[26]

The standard empirical analysis of thermograms includes an analysis of the $T_{50\%}$ parameter, which represents the temperature at which the residual mass fraction of the polymer drops to 50% (of the initial mass).[27–29] The dependence of $T_{50\%}$ on the weight fraction of SWNTs for various heating rates, for the samples degraded in the air is shown in Figure 2. It is noticed that $T_{50\%}$ is increasing slowly as the loading by SWNTs is increased and is shifted towards higher temperatures as the heating rate is raised. The dependence of the parameter $T_{50\%}$ versus the loading by SWNTs (in the range of 1%–10% wt.) is almost linear, with a slope of about 0.60°C/(% wt.). The increase of $T_{50\%}$ as the loading by SWNTs is increased may be assigned to the effect of the nanofiller and/or to the formation of an interphase between the nanotube and PO chains. As $T_{50\%}$ implies temperatures below 520°C, it is concluded that the thermo-oxidative degradation of SWNTs remains negligible and consequently solely the pristine polymer and the interphase polymer-SWNTs are contributing to this moderate increase in thermal stability (because at this temperature SWNTs are not fully oxidized and volatilized). The protecting role of SWNTs is revealed by the increase of $T_{50\%}$ as the concentration of SWNTs in the nanocomposite is increased.

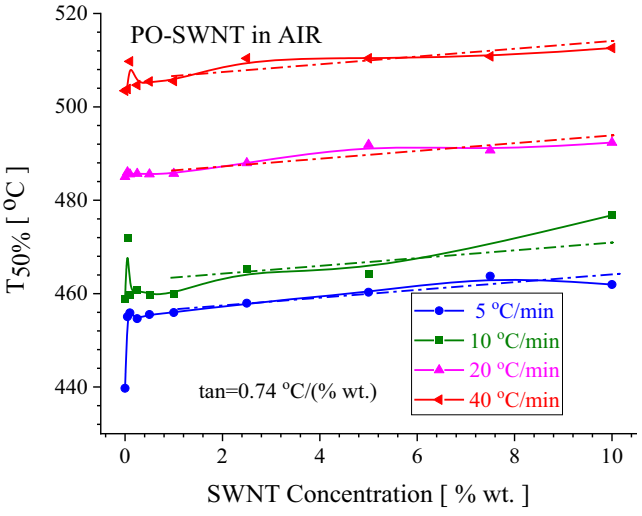

FIGURE 2 The dependence of $T_{50\%}$ on the single wall carbon nanotubes (SWNTs) content for various heating rates. [Color figure can be viewed at wileyonlinelibrary.com]

Similar parameters such as $T_{x\%}$ (representing the temperature at which the residual mass of the sample is x% of the initial mass)[27,29] were also used. Some authors identify the temperature at which 5% of the sample is volatilized ($T_{5\%}$) as the onset temperature.[30] The use of $T_{5\%}$ as an onset temperature assumes that the polymer does not contain volatiles or water molecules. The temperature at which 85% of the mass of the sample was volatilized ($T_{85\%}$) was considered. For the consistency of this analysis, $T_{5\%}$ and $T_{85\%}$ will be briefly scrutinized.

Figure 3a–d depict the dependence of the $T_{5\%}$ and $T_{85\%}$ on the loading by SWNTs, for the thermal degradation of PO-SWNTs under air atmosphere. It is noticed that the $T_{5\%}$ increases as the concentration of SWNTs is increased, for a heating rate of 5°C/min. Higher heating rates showed a complex behavior (increase at low loading by nanofiller followed by a decrease at larger concentrations of SWNTs). As $T_{5\%}$ is potentially affected by the presence of volatiles and absorbed vapors/gases, it is suggested that this is not a reliable parameter.

The $T_{85\%}$ parameter shows (see Figure 3f) a consistent increase as the heating rate is increased for all weight fractions of SWNTs. This may reflect the formation of an interphase between the SWNTs and PO, as higher temperatures are required to volatilize 85% of the nanocomposite. $T_{85\%}$ increases as the heating rate is increased. This quasi-linear dependence is characterized by a slope of about 1.87 min. For the PO-SWNTs, a degradation window may be defined by ($T_{85\%}$–$T_{5\%}$). The dependence of the degradation window ($T_{85\%}$–$T_{5\%}$) on the concentration of SWNTs for different heating rates is shown in Figure 3e. It is noticed that the degradation window becomes wider as the loading by SWNTs is increased. To conclude, the nanofiller shifts the thermograms towards higher temperatures and broadens the degradation window.

Figure 4a represents the dependence of the residual mass fraction (for $T = 950$°C) of PO-SWNT nanocomposites with various weight fractions of SWNTs, at different heating rates, thermally degraded in air. Thermal degradation of the pristine polymer in air produced a negligible amount of char (about 0.5% of the mass of the sample), which is within the experimental errors of the instrument. As SWNTs should have been completely oxidized at 950°C, the increase of the residual mass fraction of the nanocomposite as the loading with SWNT is increased indicates a residue with very high thermal stability resulting from the carbonization of PO-SWNTs nanocomposite. As expected, the residue fraction increases as the concentration of SWNTs is increased (see Figure 4a), suggesting the formation of an interphase.

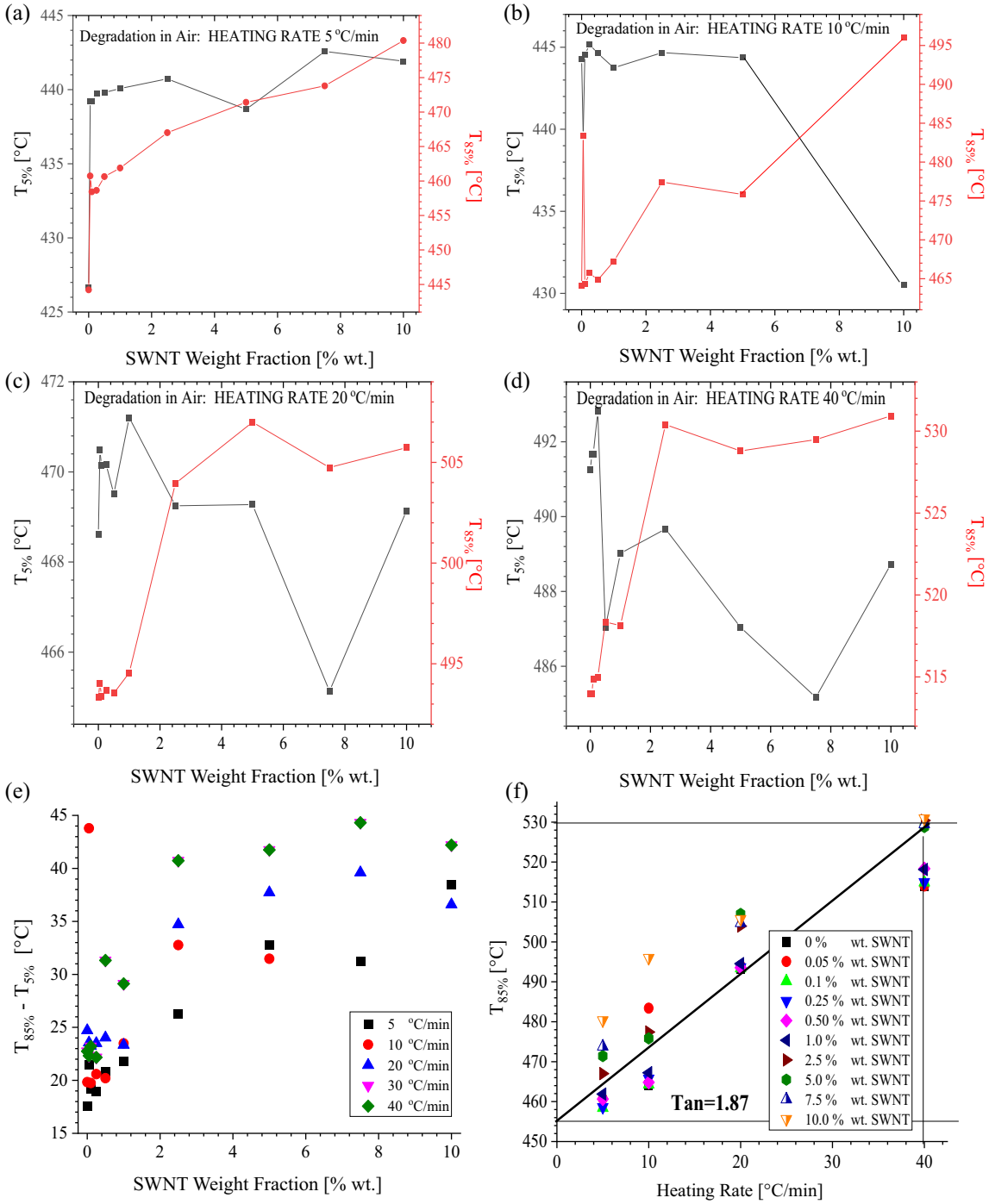

FIGURE 3 (a–d) The dependence of $T_{5\%}$ and $T_{85\%}$ on the loading with single wall carbon nanotubes (SWNTs) at different heating rates. (e) The dependence of the degradation window ($T_{85\%}$–$T_{5\%}$) on the concentration of SWNTs for different heating rates. (f) The dependence of $T_{85\%}$ on the heating rate for different loadings by SWNTs. [Color figure can be viewed at wileyonlinelibrary.com]

However, the residual mass at 950°C, while not negligible is not sufficiently large to allow for a reliable quantitative measurement. The conclusion regarding the formation of an interphase is merely qualitative as no quantitative information may be extracted.

In some cases, residues frequently assigned to catalysts' impurities were reported at such high temperatures.[31,32] To be safer, a temperature $T_{950}^{(Air)}$ was introduced to quantify the residual mass fraction for PO-SWNTs nanocomposites subjected to thermal degradation in air, up to 950°C. An almost complete thermal degradation (in air) of purified carbon nanotubes was reported at slightly lower temperatures (at 850°C).[32–34] Hence the parameter $P^{(Air)}$ representing the residual mass

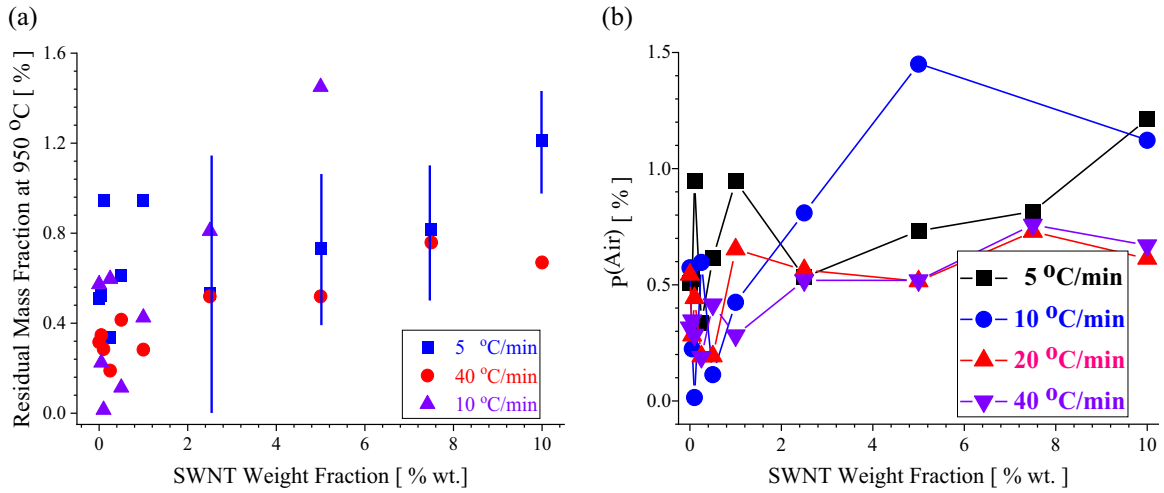

FIGURE 4 (a) The dependence of the residual mass fraction of the nanocomposite at 950°C on the weight fraction of single wall carbon nanotubes (SWNTs), at different heating rates, for samples degraded in air. (b) Represents the dependence of $P^{(Air)}$[%] on the weight fraction of SWNTs for different heating rates. [Color figure can be viewed at wileyonlinelibrary.com]

fraction of the sample at 950°C may provide additional information about the thermal oxidative degradation:

$$P^{(Air)}[\%] = 100 \times \frac{M^{950}}{M^{100} - M^{950}} = \frac{100}{\frac{M^{100}}{M^{950}} - 1} \quad (1)$$

where M^{100} is the (residual) mass of the sample at 100°C and M^{950} is the residual mass of the sample at 950°C. The mass M^{100} includes the polymer, the nanofiller, and the interphase. The lowest temperature was selected at 100°C, to eliminate the contribution of eventually labile products. Neither the polymer nor the filler is expected to degrade in the temperature range from room temperature to 100°C.

For the pristine (PO) samples degraded in air, the residual mass at 950°C represents about 0.3–0.5% wt. and shows a weak dependence on the heating rate (see Figure 4b). The SWNTs are volatilized in this oxygen-containing atmosphere. Previous research indicated that highly purified HIPCO SWNTs are almost completely volatilized at 950°C.[25]

If the volatilization of the sample at 950°C would have been completed, then $P^{(Air)}$ would be equal to zero irrespective of the heating rate or SWNTs content. As seen in Figure 4b, the residual mass fraction during air degradation, $P^{(Air)}$ [% wt.], shows a weak increase as the loading with SWNTs is increased, suggesting the formation of an interphase with high thermal stability (that is not degraded thermally in the air up to 950°C). Authors suggest that measured residual mass at 950°C, in the air atmosphere suggests the formation of an interphase but that the data is not sufficient to demonstrate and quantify this interphase due to the experimental errors. As similar results were obtained at different heating rates, it appears fair to conclude that the presence of an interphase is demonstrated and that this interphase represents about 1% of the mass of the sample for a loading of about 7.5% SWNT and a low heating rate (5°C/min). This reasoning is reinforced by observing that the pristine polymer as well as the SWNTs are expected to be completely volatilized at 950°C. Nevertheless, is important to notice that a precise quantitative estimation is not possible unless the concentration of the filler is significantly increased. The thermal degradation in air exhibits a weak component at large loading with SWNTs and a high heating rate that was assigned to the degradation of the nanofiller but may eventually also include some other contributions. Some of these concepts ($T_{x\%}$) are purely conventional and do not have a solid theoretical basis, being criticized by several authors.[25]

At this point, the standard analysis of the TGA data is almost completed. The dependence of the residual mass in air and of the $T_{50\%}$ parameter (in air) on the loading by SWNTs, for different heating rates, suggested the formation of an interphase between the polymeric matrix and the nanofiller. However, except for this qualitative outcome, the standard TGA analysis cannot provide quantitative information regarding the interphase.

3.2 | Thermogram's derivative analysis or brief derivative defines the derivative of the thermogram with respect to the temperature

Modern TGA instruments can record the derivative (hardware). Alternatively, the derivative may be obtained

by the software. All derivatives' data analyzed in this manuscript were recorded by using the TGA's spectrometer hardware. Recently more and more authors have focused on a more detailed analysis of the thermal degradation data. One of the most frequently used improvements starts from the observation that in many cases the degradation is represented by a single sigmoid (or a linear combination of several sigmoids). Mathematically, this function has no extremum points but presents a (single) inflection point. For a symmetrical sigmoid-like thermogram taking values between 0 and 100, the inflection point (temperature) is located precisely at a temperature defined as $T_{50\%}$, with an amplitude of 50 mass units. As the inflection point is not easy to locate on the real thermogram, the mathematical analysis revealed that a simple derivation with respect to the temperature converts the inflection point (of the thermogram) into an extremum point. Thus, for ideal thermograms, the inflection temperature T_{inf} is expected to be identical to $T_{50\%}$. T_{inf} has a deeper significance representing the temperature at which the residual mass (or residual mass fraction) loss rate is highest. Technically the derivative of the thermogram versus temperature shows a minimum at the inflection temperature. By multiplying the residual mass loss rate by "–1" this minimum is converted into a maximum. All derivatives of the thermograms considered in this paper show the inflection temperature as a maximum. Hence, TGA analysis started to include the derivatives of the as obtained thermograms, thus improving this experimental technique.

The first-order derivatives of the thermograms (versus temperature), for the PO-SWNTs degraded under nitrogen atmosphere, are collected in Figure 5a–d. It is observed that all thermograms look similar, with a

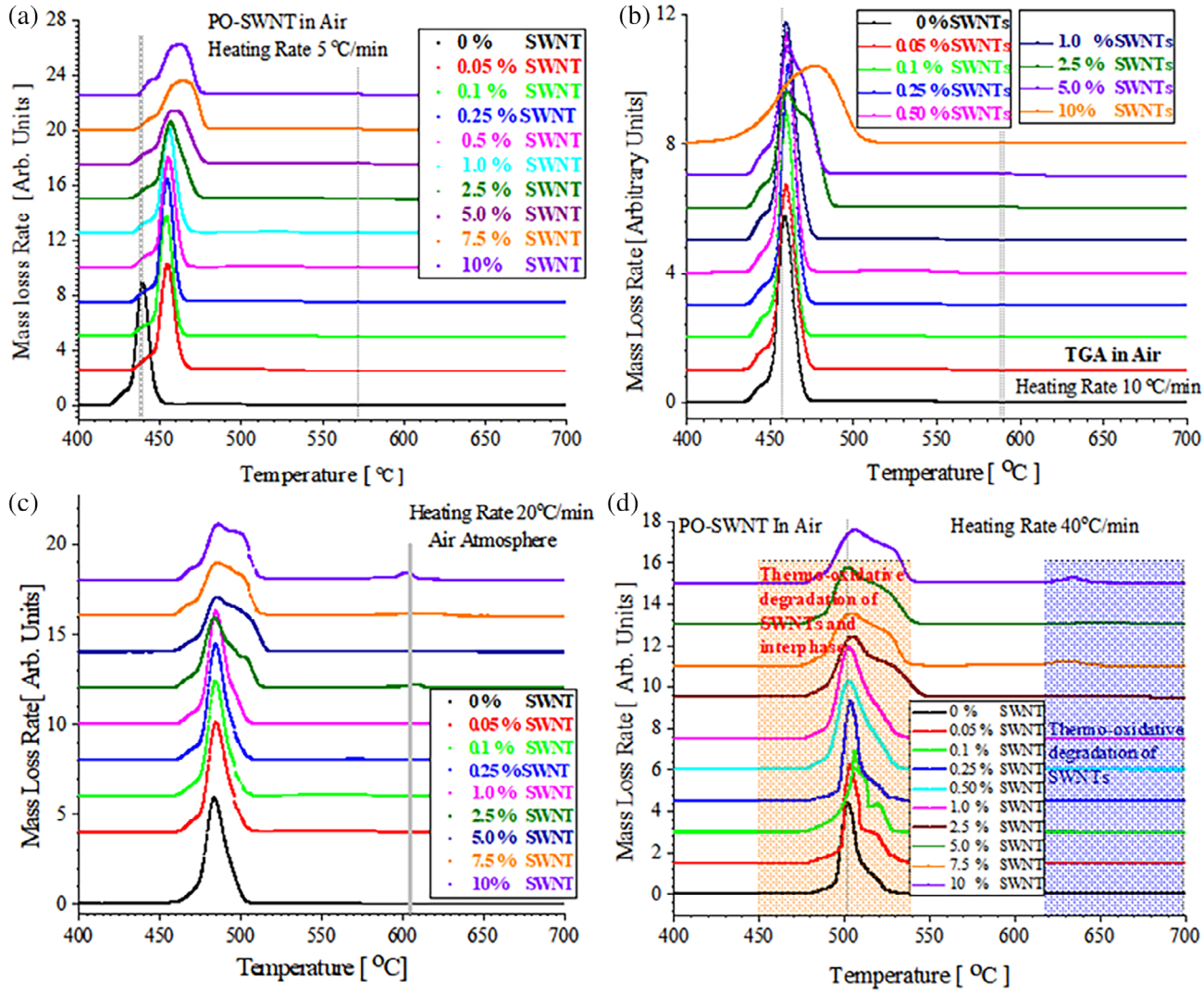

FIGURE 5 (a–d) Detail of the first order derivatives of the thermograms of polyoctenamer-single wall carbon nanotubes (PO-SWNTs) nanocomposites at various heating rates and loading by SWNTs, in air. [Color figure can be viewed at wileyonlinelibrary.com]

central peak located at about 500°C. No significant thermos-oxidative degradation was noticed below 400°C.

For better visualization of the thermal degradation in air, the thermograms are zoomed on the temperature range 400–700°C. Pristine PO derivatives exhibit a single dominant Lorentzian shape line with weak contributions to the left (lower thermal degradation temperatures) of the most intense peak at low heating rates. This weaker degradation is shifted to higher temperatures, as the heating rate is increased. The weak degradation was assigned to competing thermal degradation processes involving potential low molecular compounds. The addition of SWNTs complicates the temperature dependence of the derivative. As the loading with SWNTs was increased, the main peak associated with the thermal degradation in the air of the polymer shifted to higher temperatures and broadened. This is better noticed at low heating rates and reflects the contribution of the interphase (see Figure 5a–d).

At heating rates higher than 10°C/min, for nanocomposites loaded by more than 1% wt. SWNTs, a broad peak of the residual mass fraction loss rate versus temperature was noticed. Here, the contribution of the interphase is obvious. At high concentrations of SWNTs (above 2% wt.) the oxidation of SWNTs is noticed at temperatures above 500°C. This peak was shifted to a higher temperature (up to about 625°C) as the heating rate was increased (and was not observed in pristine PO at any heating rate), thus justifying its assignment to the oxidation of SWNTs. The mass loss rate becomes negligible above 700°C for all samples. It is concluded that the main degradation peak represents the thermos-oxidative degradation of the polymer, with contributions from the thermos-oxidative degradation of the interphase of PO-SWNTs.

To conclude, most thermo-oxidative degradation processes occur between 400 and 700°C. However, for PO-SWNTs, this domain is divided into a high-temperature component, typically between 550 and 700°C, where the thermo-oxidative degradation of SWNTs becomes dominant and a low-temperature thermo-oxidative region, which extends from 400 to 550°C and is dominated by the degradation of the polymer and of the polymer-SWNTs interphase (see Figure 5d).

The overall "polymeric" thermo-oxidative degradation process in the temperature window 400 to 550°C was simulated by assuming two overlapping generalized Lorentz-like dependencies. Mathematically, the following fitting function has been used in Origin 9.0:

$$\begin{aligned} Y(T) &= \mathrm{dM}(T)/\mathrm{dT} \\ &= (2I_1/\pi)\left[W_{I1}/4\times(T-T_{I1})^2+4{W_{I1}}^2\right] \\ &\quad + (2I_2/\pi)\left[W_{I2}/4\times(T-T_{I2})^2+4{W_{I2}}^2\right]+Y_0+\mathrm{LT} \end{aligned} \tag{2}$$

where $Y(T)$ is the overall (bulk polymer plus polymer in interphase) residual mass loss rate at the temperature T, M is the residual mass fraction of the nanocomposite at a given temperature, T, Y_0 is a constant that controls the baseline correction (which include the mass fraction of SWNTs as it is not affected by the thermos-oxidative degradation within the range of temperatures considered), and L is the slope correction. I_1, and I_2 are the amplitudes of the Lorentz-like lines centered at their inflection temperatures labeled as T_{I1} and T_{I2}, and characterized by their width W_{11} and W_{I2}. The fit of the dominant degradation process performed using Equation (2) was good, with correlation coefficients better than 0.95 for all best fits. Figure 6a provides an example of this fit over the temperature range of interest for the thermo-oxidation of the polymeric components, for the PO-SWNTs nanocomposites heated at a rate of 5°C/min. As shown in Figure 6b, the widths of both degradation processes (identified as W_{I1} and W_{I2} in Equation (2)) increase as the heating rate is increased, in agreement with the dependence of the temperature window $T_{85\%}$–$T_{5\%}$ (Figure 3e) and of $T_{85\%}$ (Figure 3f) on the heating rate. Figure 6c represents the dependence of the inflection temperatures T_{I1} and T_{I2} on the weight fraction of SWNTs, for the samples thermally degraded at 5°C/min. Up to a multiplicative scale factor, the two dependencies (T_{I1} and T_{I2} on SWNTs loadings) are similar.

To conclude the (temperature) derivatives of thermograms support qualitatively the formation of the interphase but do not allow any quantitative estimations.

3.3 | Estimating the interphase fraction from TGA data

The most important task is to obtain a quantitative description of the polymer-nanofiller interphase. To achieve this, it is important to notice that the focus is on the two-component polymeric system consisting of the bulk polymeric matrix and the polymer immobilized within the interphase. It is expected that the strongest degradation process is associated with the degradation of the polymeric matrix in interaction with the nanofiller. In the case of PO-SWNTs, this process has an inflection temperature T_I. Based on the analysis of the thermograms' derivatives, it is concluded that $T_{I2} = T_I$. The dependence of T_I on the loading with SWNTs is considered an outcome of the presence of the interphase.

The bulk polymer is characterized by the inflection temperature $T_I^{(0)}$. The polymer loaded by x% wt. SWNTs have an inflection temperature, $T_I^{(X)}$, where: $T_I^{(X)} \geq T_I^{(0)}$. It was noticed that the inflection temperature depends on the loading by SWNTs. Hence, a fictive inflection

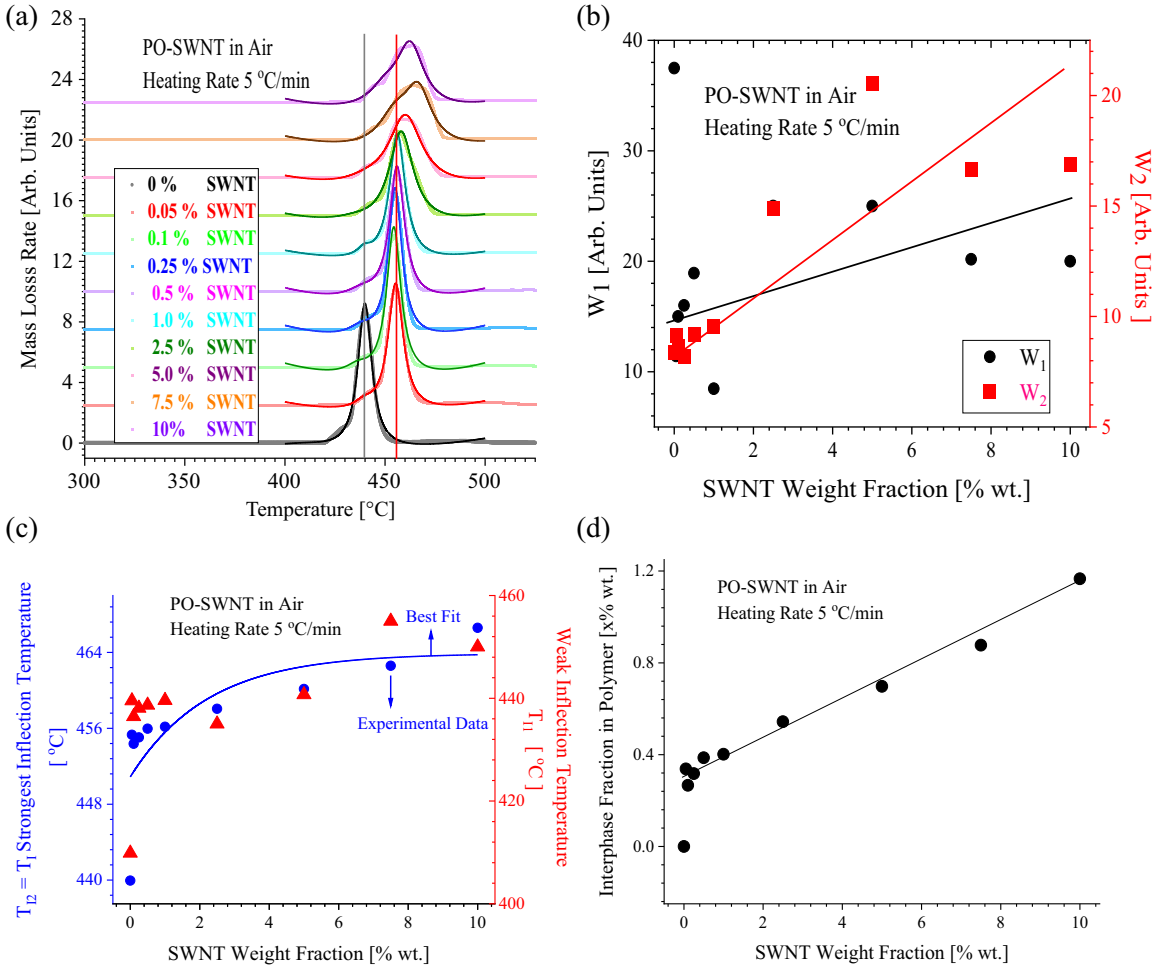

FIGURE 6 (a–d) The best fit for the thermo-oxidative degradation of polyoctenamer-single wall carbon nanotubes (PO-SWNTs) at a heating rate of 5°C/min, at various loadings by SWNTs. The thin line/dot represents the recorded thermograms. Darker bold lines represent the best fit obtained by using Equation (2). (b) The dependence of the inflection temperatures on the loading by SWNTs for the two thermo-oxidative degradation processes. (c) The dependence of the interphase weight fraction on the weight fraction of SWNTs. [Color figure can be viewed at wileyonlinelibrary.com]

temperature $T_I^{(\mathrm{INTERPHASE})}$, assigned solely to the filler may be calculated by using the expression:

$$T_{(I)}^{(x)} = T_I^{(0)} + \left(T_I^{(\mathrm{INTERPHASE})} - T_I^{(0)}\right)(1 - \exp(-\alpha x)) \quad (3a)$$

where α is a fitting constant. For $x = 0$ (i.e., no filler), $T_I^{(x)}$ degenerates into $T_I^{(0)}$, as expected. For $x \to \infty$, $T_I^{(x)} \to T_I^{(\mathrm{INTERPHASE})}$. Please notice that the fictive inflection temperature of the interphase is obtained as $x \to \infty$. Formally this indicates that the inflection temperature of the nanofiller corresponds to the situation in which the fraction of the nanofiller is ∞. In most cases, this is just theoretical reasoning, as the inflection temperature of the filler may not be always available or easy to determine.

Here, $T_I^{(\mathrm{INTERPHASE})}$ is the inflection temperature for the pure 100% interphase, associated with the strongest sigmoid in this study. This is a theoretical concept at the boundary where the amount of polymer in the bulk is disappearing. Defining this limit, it is very important to observe that $T_I^{(\mathrm{INTERPHASE})}$ does not exist if there is not at least one polymeric segment in the interphase. Consequently, x is strongly related to the nanofiller. Somehow, due to the separate measurements of the 2 sigmoids, it is recognized that the thermal degradation in the air of PO-SWNTs deconvolutes the thermal degradation of the polymer component (including polymer interphase) from the thermal degradation (oxidation) of SWNTs. The best fit of Equation (3a) for the samples degraded in air, at a heating rate of 20°C/min, as a function of SWMTs loading is shown in Figure 6c. The parameters corresponding to the best fit are $T_I^{(0)} = 451°\mathrm{C}$, and $T_I^{(\mathrm{INTERPHASE})} = 464°\mathrm{C}$.

$T_I^{(\mathrm{INTERPHASE})}$ together with $T_I^{(0)}$ and $T_I^{(x)}$ as well x are all connected to both the polymer and the

nanofiller, at least at extreme limits such as very low or very large loadings. The sigmoid representing the thermal degradation (oxidation) of SWNTs is weaker because the loading by SWNTs was relatively low (at most 10% wt.). Additional factors may contribute to the broadening of the width of the SWNTs degradation. Such a detailed study would require samples with a larger concentration of nanotubes.

Hence, it appears reasonable to use a simple analogy to the glass transition in miscible polymeric binary blends. This approach implies that the bulk polymer and the polymer trapped in the interphase are perceived as a compatible blend of 2 miscible polymers. As the only quantifiable parameter is the inflection temperature, it will be assumed that the actual inflection temperature of the polymer nanocomposite $T_I^{(x)}$ depends on the inflection temperature of the pristine polymeric matrix $T_I^{(0)}$ and the inflection temperature of the interphase $T_I^{(\text{INTERPHASE})}$ according to a Fox like equation[35,36]:

$$\frac{1}{T_I^{(x)}} = \frac{1-x^{(I)}}{T_I^{(0)}} + \frac{x^{(I)}}{T_I^{(\text{INTERPHASE})}} \tag{3b}$$

where x ($x = x^{(I)}$) is the weight fraction of the interphase in the polymeric component. For $x^{(I)} \to 0$ (no nanofiller) it is obtained $T_I^{(x)} \to T_I^{(0)}$, as expected. For $x^{(I)} \to 1$ it is obtained $T_I^{(x)} \to T_I^{(\text{INTERPHASE})}$, as expected. To conclude, the proposed analogy satisfies reasonable asymptotic behavior. At the extreme theoretical limit at which the pure 100% interphase has an infinitely large inflection temperature $T_I^{(\text{INTERPHASE})} \to \infty$, it is obtained $T_I^{(x)} = T_I^{(0)}/x^{(I)}$, where $x^{(I)}$ would range between 0 and 1. Because $x < 1$ this demonstrates that the nanofiller increases the inflection temperature of the polymeric matrix. However, the highest thermal stabilization would appear at very small values of $x^{(I)}$.

At this point, it is obvious that Equation (3b) relates the inflection temperature of the polymer nanocomposites to the inflection temperature of the pristine polymer through the volume fraction of the interphase in the whole polymeric system.

It is important to notice that this approach did not include the possible effect of the thickness of the polymer on the inflection temperature (as the parallel to the glass transition phenomenon suggests[37]), and neglected the contribution of the nanofiller to the degradation process, in the sense that the total mass of the interphase added to the mass of the bulk polymer is equal to the total polymeric mass (i.e., no atoms of the nanofiller where added to the interphase).

However, in the case of degradation in air, the local degradation of SWNTs although small is not negligible. Under these circumstances, the use of the Gordon and Taylor or Kwei[35] equations may provide an additional layer of accuracy. These equations may be derived (and better understood) within the free volume approximation.[38]

This preliminary study will restrict the analogy between the polymer blend and the two polymer-containing components (matrix polymer and interphase polymer) to Equation (3b), which allows for a simplified estimation of the interphase volume fraction:

$$x^{(I)} = \frac{T_I^{(\text{INTERPHASE})}\left(T_I^{(x)} - T_I^{(0)}\right)}{T_I^{(x)}\left(T_I^{(\text{INTERPHASE})} - T_I^{(0)}\right)} \tag{4}$$

It is noticed that the inflection temperature of the extrapolated interphase ($T_I^{(\text{INTERPHASE})}$) is larger than the inflection temperature of the polymer $T_I^{(0)}$ and that the inflection temperature of any nanocomposite loaded by x% vol ($T_I^{(x)}$) is greater than the inflection temperature of the polymeric matrix ($T_I^{(0)}$). This demonstrates that actually, x ranges between 0 and 1.

At this point, it is possible to estimate the fraction of the interphase x if the temperatures $T_i^{(x)}$, $T_i^{(0)}$, and $T_i^{(\text{INTERPHASE})}$ are determined. $T_i^{(0)}$ is the inflection temperature of the pristine polymer (no filler) determined from the thermogram of the pristine polymer. The inflection temperature $T_i^{(\text{INTERPHASE})}$, is not always directly accessible. In some cases, the thermogram of the filler can be recorded and this temperature can be directly accessible. In the case when this temperature is not directly accessible, it will be estimated by the extrapolation of the inflection temperature versus the concentration of nanofiller (to the theoretical situation of 100% nanofiller). This typically requires a set of at least 5–6 thermograms of the same nanocomposite with various concentrations of the nanofiller. Finally, $T_I^{(\text{INTERPHASE})}$ is the inflection temperature for the interphase of a polymer-based nanocomposite load by a nanofiller. In the case of the PO-SWNT nanocomposite considered here, $T_i^{(\text{INTERPHASE})}$ was determined by fitting the Equation (3a). The best fit, together with relevant data is included in Figure 6b. Figure 6c depicts the dependence of the weight fraction of the interphase on the loading with SWNTs. It is noticed that the interphase fraction $x^{(I)}$ associated with the polymer increases as the loading by the nanofiller is increased. These preliminary studies provide a simple path to estimate the fraction of the interphase within polymer-based nanocomposites. For simplicity, it was supposed that the volume fractions are equal to the mass fractions; however, the qualitative dependence and results are not affected by this approximation.

4 | COMPLEMENTARY DATA

The WAXS spectra of PO-SWNTs composites are a superposition of the lines originating from the crystallites of the polymeric matrix and the SWNTs lines (see Figure 7a). As reported elsewhere the strongest line originating from SWNTs is located at about 26° (in two theta) corresponding to (002) nanotube reflection planes.[39,40] The other less intense and wider lines were reported in SWNTs at 42 and 56° respectively, corresponding to the (100) and (004) reflections. The positions of these lines are marked in Figure 7a, although they are barely visible. The most intense peak of SWNTs is consistent with not strongly aligned SWNTs,[40] as expected for the samples investigated, thus suggesting a good dispersion of SWNTs.

From Figure 7a it is noticed that the addition of SWNTs does not change the positions of the lines originating from PO. Consequently, it may be concluded that the crystalline symmetry and the size of the unit cell of PO crystals are not affected by the loading with SWNTs. As the line widths of the spectra assigned to the polymeric matrix do not change significantly, it is concluded that the size of the PEO crystallites is not affected by the loading with SWNTs.

Figure 7b collects the Raman spectra, obtained by using a red excitation (785 nm) for all PO-SWNTs samples. As expected, both the contributions of nanotubes and the polymer are sensed. Raman spectroscopy is extremely efficient in monitoring the local motions of small groups of atoms and molecules such as bending, stretching, wagging, and so forth.

Figure 8a focuses on the Raman spectra for small shifts, ranging between 100 and 300 cm^{-1}. It is interesting to notice the presence of three weak and broad modes in this range, originating from the polymer and assigned to the elastic features of the polymer. The doping by SWNTs rapidly replaces these modes with typical lines originating from SWNTs. The line noticed in the range 150–165 cm^{-1} was assigned to the radial breathing mode (RBM) of the nanotube. This line exhibits a weak shift to larger Raman shifts as the concentration of SWNT is increased, suggesting that the nanotubes are distorted and eventually do not close seamlessly in a cylinder at low concentrations of nanofiller. It was shown that the increase of the position of the RBM mode as the SWNTs content is increased reflects a decrease in the diameter of SWNTs,[41] due to strong interactions. The increase of nanofiller concentrations facilitates the healing of nanotubes, as they are transiting to an ideal tube. The radial tangential mode (RTM) mode has a complementary behavior exhibiting a decrease of the Raman shift as the concentration of nanotubes is increased. The nanotubes responsible for this mode exhibit further departures from the ideal smooth cylinder, with shape deviations towards a helix geometry and potential opening of the nanotube. Such dependence suggests a transition from a tube in the 2nd RTM mode towards a helix in the first RTM mode.[42] The distortions of the cylindrical SWNTs to a helix shape and the potential opening of the nanotubes should occur at the interphase between the polymer and the nanofiller and should express strong interactions. As shown in Figure 8b, the position of RTM modes is shifting towards lower values as the carbon nanotube loading is increased, thus revealing an increase in the nanotube diameter. This strong shape distortion originates from C–C stretching vibrations within the SWNTs[42] and eventually between C atoms of the polymer

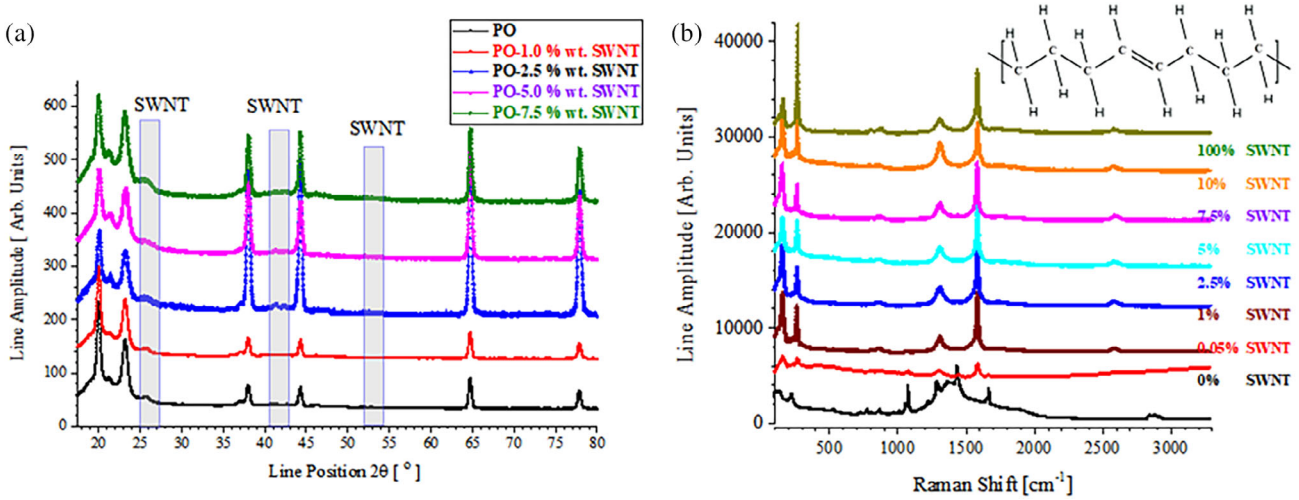

FIGURE 7 (a) The wide-angle x-ray scattering spectra of polyoctenamer-single wall carbon nanotubes (PO-SWNTs) nanocomposites (left panel). (b) The Raman spectra of PO-SWNTs nanocomposites (right panel). [Color figure can be viewed at wileyonlinelibrary.com]

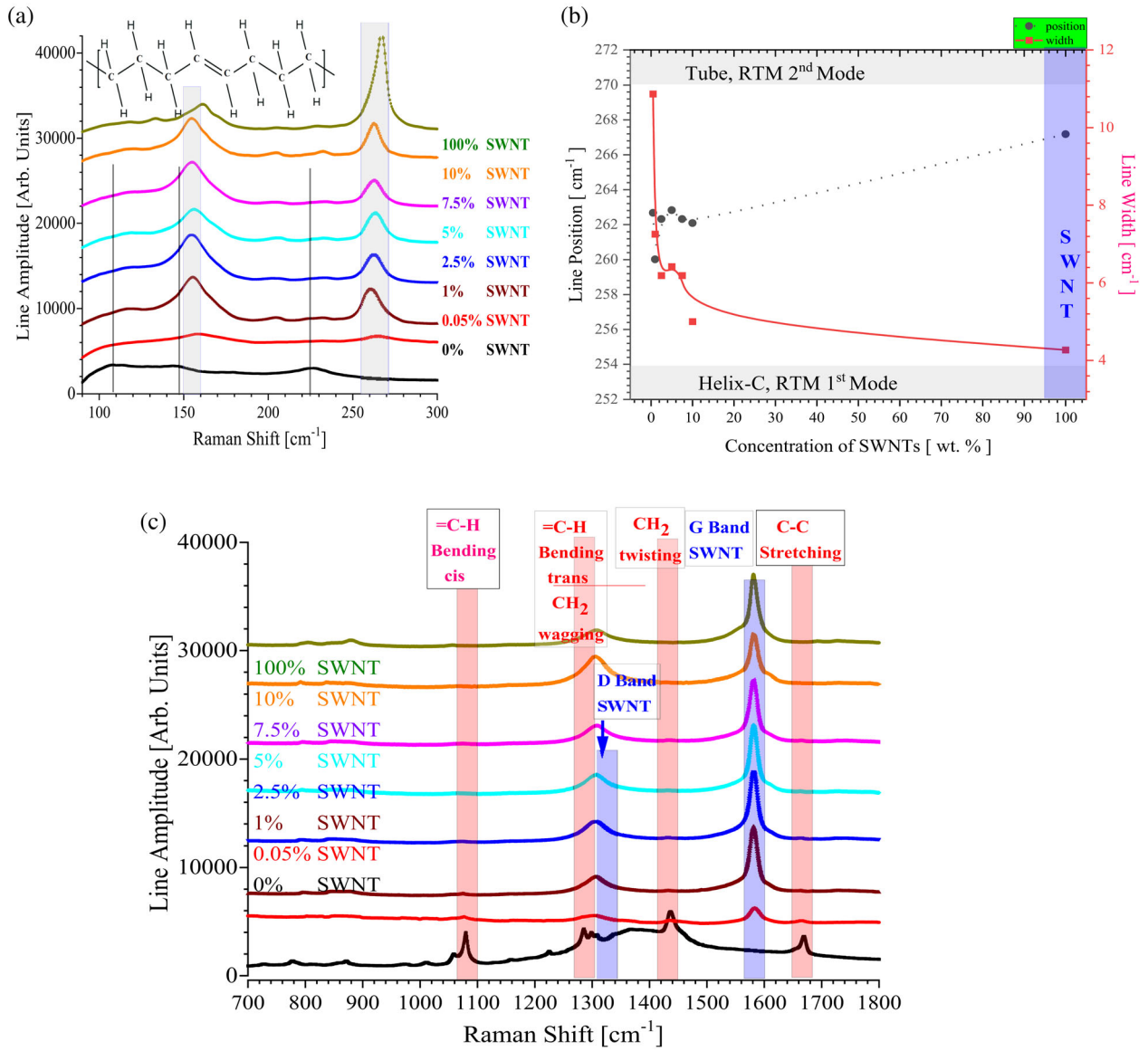

FIGURE 8 (a) Left top panel. Detail of Raman spectra in the radial breathing mode (RBM) and RTM modes range, for polyoctenamer-single wall carbon nanotube (PO-SWNT) nanocomposites. (b) Right top panel. The dependence of Raman line position and widths for the RTM mode. (c) Lower panel. Middle range Raman spectra of PO-SWNTs nanocomposites. [Color figure can be viewed at wileyonlinelibrary.com]

that wandered remarkably close to the nanotube and C atoms located on the nanotube.

The D line of SWNTs (associated with defects) was noticed within the expected range of Raman shifts[41] (at about 1305 cm^{-1} compared with the reported value of about 1351 cm^{-1}), suggesting strong interactions. The main G line (associated with graphite structures) is located at 1581 cm^{-1} and is almost not affected by the loading with SWNTs. This value is an average between G + and G– for helix (opened) nanotubes. The G′ (or 2D) band is observed at 2580 cm^{-1} [41] and was reported to be associated with strong sp^3 C–H bonds involving the edges of the helix-distorted nanotube.[42] While these data were reported in hydrogenated SWNTs, we do suggest that this double resonance confirms strong C–H bonds between the C atoms (located on the edges of nanotubes) and the H atoms of the polymeric matrix. The central components of the Raman spectrum, for Raman shifts ranging from 700 to 1800 cm^{-1} are shown in Figure 8c. The main molecular motions occurring within the polymeric matrix are indicated on the corresponding Raman lines. The pristine polymer has a dominant trans structure with less than 20% cis components. As noticed in most polymer-carbon nanotube nanocomposites, the nanofiller freezes the molecular motions of the polymeric matrix. The sudden disappearance of the Raman lines assigned to the

polymeric matrix demonstrates the strong interaction between the polymer and the nanotubes. This concludes that the interphase between the PO and SWNTs is built on an immobilized (frozen) polymer backbone that eventually involves C–H bonds between the polymer and its matrix.

Additional DSC data has been collected for 2 significant samples. The first one is identified as pristine PO. This sample contains no nanofiller but was subjected to the same thermomechanical treatment (melt mixing) as all nanocomposites belonging to the series PO-SWNTs discussed here.

The DSC was programmed to perform several cycles consisting of heating from −55 to 150°C and cooling from 150 to −55°C. At the end and the beginning of each cycle, a 3-min isothermal was included. Three full heating–cooling cycles were scheduled. The philosophy for this design is the following: The first heating rate relaxes the potential stresses and strains frozen after the mixing step, erasing the so-called mechano-thermal history of the sample. Thus, in the first heating step, both the crystalline phase as well as the relaxation of strains and stresses are relaxed. The second heating step would record the equilibrium melting temperature of the sample. However, as it is not obvious that the sample's history was erased, a third confirmation heating cycle was considered. The experimental data are deemed reliable if the second and third cycles are identical.

From Figure 9a, b, it is noticed that the second and third cycles are overlapping, supporting the reliability of these experimental data for both pristine PO as well as for PO-10% wt. SWNTs.

In the case of pristine PO (subjected to the thermomechanical processing), the heat flow for the first cycle shows a broad melting temperature located at about 57.8°C (see Figure 9a). Upon heating, the second heat flow reveals a narrower melting process located at about 56.5°C. The narrowing of the melting transition and the shift of the melting temperature from 57.8 to 56.5°C reflects the erasing of the thermal history of the sample. As mentioned earlier, the third heating overlaps perfectly with the third one, confirming the complete removal of the thermal history.

For PO loaded by 10% SWNTs (see Figure 9b), the first heating shows a complex shape with two minimums suggesting two overlapping melting temperatures. The lower melting temperature labeled as $T_M^{(1)}$ (see Figure 9b), located at 54°C, was tentatively assigned to the polymer. The high melting temperature $T_M^{(2)}$ (see Figure 9b), located at 61.5°C was assigned to the polymer trapped within the interphase. Strong local stresses and/or strain within the polymeric phase are responsible for the splitting and shift of the melting temperature. However, the second heating reveals a unique melting process, characterized by a melting temperature of 55.6°C. During the first heat, the stresses and strains indicated earlier are melted. The severely distorted polymer-nanotube interphase collapsed into a thermodynamically relaxed structure. However, the melting temperature (at equilibrium after the first heat) is noticed at 55.6°C compared to 56.5°C noticed in the pristine polymer after the first heating. This shift of the melting temperature reveals the existence of a thermal equilibrium interphase, showing that a certain amount of polymer remains glued

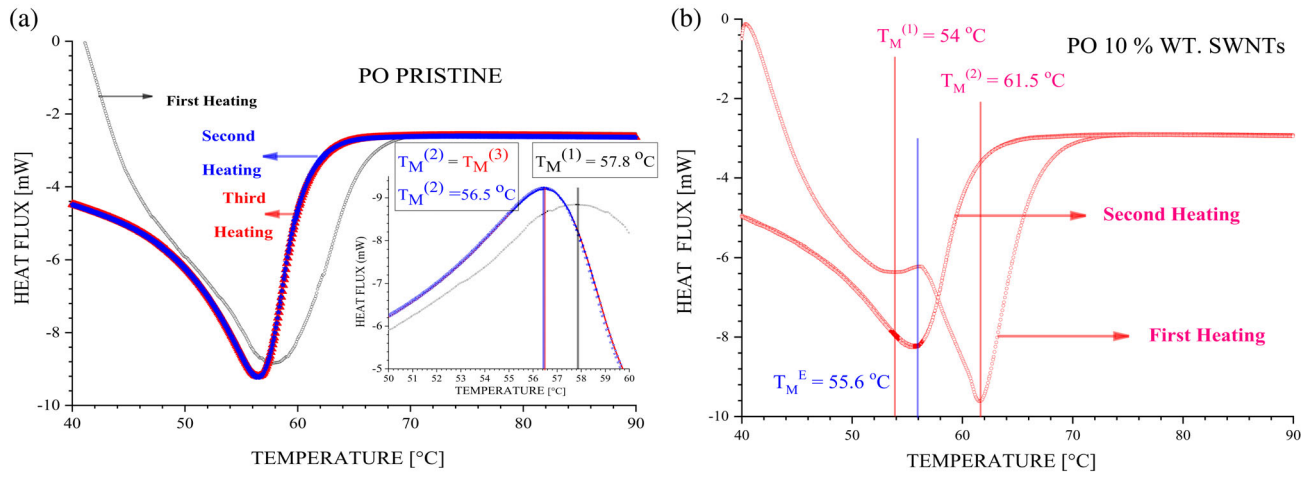

FIGURE 9 (a) Left panel. The differential scanning calorimetric (DSC) spectra of pristine polyoctenamer (PO) around the melting temperature for the first heating (cycle 1), second heating (cycle 2), and third heating (cycle 3). It is noticed that the second and third cycles overlap. (b) Right panel. The DSC spectra of PO-SWNTs loaded by 10% wt. SWNTs around the melting temperature for the first heating (cycle 1), second heating (cycle 2), and third cycling (left panel). It is noticed that the second and third cycles overlap. [Color figure can be viewed at wileyonlinelibrary.com]

to the nanofiller. Moreover, by observing that the equilibrium melting temperature for the polymer loaded by SWNTs is closer to the melting temperature of the polymer ($T_M^{(1)}$) is concluded that the weight fraction of the polymer is larger than the weight fraction of SWNTs. This generates additional support for a Fox–Flory-like process.

5 | DISCUSSIONS AND CONCLUSIONS

This study focused on the isothermal degradation in the air of polymer-based nanocomposites, namely PO-SWNTs. The main outcomes of this research are:

1. A standard analysis of TGA data and results based on the analysis of the as-recorded thermograms that supports (solely qualitatively the formation of an interphase).
2. A clear discrimination between the interphase concept (which implies a non-zero thickness and consequently non-zero volume and mass) and interface (defined as a separation surface of zero thickness and consequently characterized by zero volume and mass).
3. A more detailed analysis of the temperature derivative of the thermograms was presented.
   a. It was shown that the temperature derivative deconvolutes the degradation of polymer from the oxidation of nanotubes. This is expected to be the case in many polymer-based nanocomposites, where the nanofiller has significantly higher thermal (and eventually oxidative) degradation compared to the polymeric matrix.
   b. It was shown that the resolution of the thermograms' derivatives is better than the standard resolution of the thermograms.
   c. It was concluded that this approach allows the introduction of at least 3 parameters, not necessarily all new. These are the inflection temperature (which appears as a peak in the derivative) and theoretically coincides with $T_{50\%}$, the inflection mass, which should be identical to 50% of the initial mass for ideal systems, and the width of the degradation process.
   d. The inflection points receive a physical significance representing the coordinates where the mass loss rate is highest.
   e. It was shown that the inflection temperature is shifted towards higher temperatures as the loading by SWNTs is increased.
   f. It was shown that while the experimental data points (qualitatively) for the formation of an interphase a quantitative estimation (not a precise calculation!) is not possible in most cases.
4. An original approach for the estimation of the fraction of the interphase was suggested. The approach was based on the hypothesis that a Fox-like equation may be used to determine the interphase fraction. This was based on the Fox model and assumed that the polymeric matrix and the interphase behave like a blend of two compatible polymers, with one component of the blend represented by the inflection temperature for the pristine polymer and another component represented by the asymptotic inflection temperature at large content of filler. It is important to mention that the main sigmoid (degradation process) is reasoned as representing the combined effect of the thermal degradation of the polymer and the interphase, where the oxidation of SWNTs is noticed at higher temperatures separated from the polymer degradation.
5. The proposed approach allows for the estimation of the interphase of a polymer-based nanocomposites if the filler has a well-defined shape (spheres, planes, tubes) and if the nanofiller is uniformly deposited. In the case of nanofillers with irregular shape or nanofillers patched with polymers, the approach can provide the fraction of the interphase but not the thickness of the interphase.
6. Complementary support for the formation and understanding of the PO-SWNTs interphase. X-ray scattering confirms that the symmetry of the polymer and the sizes (length and angles) are not affected by the loading with nanotubes. Even more, the line widths are almost independent of the loading with SWNTs indicating that the crystallites' sizes are independent of SWNTs content. It was concluded that polymer segments located sufficiently far from the nanotubes are not affected by the loading with nanotubes, thus preserving the crystalline symmetry and crystallite build-up.
7. Raman spectroscopy provided additional support for the formation of the PO-SWNTs interphase. The analysis reveals complex and strong modifications in the geometry of nanotubes (towards helix structures) as well as increased concentration of defects and even potential descrolling of SWNTs. The combined effects of C–C and C–H interactions justify a very thin interphase wrapped around the nanofiller. Raman spectra of polymer motions revealed that the addition of SWNTs immobilizes these molecular vibrations, resulting in a rigid polymeric interphase. Further away from nanotubes, the polymer may not be affected by the presence of the nanofiller. The blend invoked within this manuscript is exactly the blend between the "immobilized polymer"

located in the neighborhood of nanotubes and the almost pristine polymer, located away from the nanotubes. Due to the strong Raman absorption of nanotubes, the Raman lines due to the polymer located away from the nanofiller are masked.

8. DSC data on pristine PO (subjected to the same thermomechanical processing as the samples loaded by SWNTs) and PO-SWNTs nanocomposites demonstrated the presence of the interphase through shifts in the melting temperatures and splitting of the melting temperature for PO loaded by 10% wt. SWNTs. These features suggest a Fox–Flory like process for melting temperatures.
9. The enhancement of thermal stability due to the addition of nanofillers is explained by the formation of an interphase between the polymeric matrix and the nanofiller. While in the general case both bonding and non-bonding interactions may contribute to the final architecture of PO-SWNTs, the experimental data do not suggest a strong bonding contribution. Due to the elemental composition of these nanocomposites, the probability of weak hydrogen bonding is low.
10. Consequently, the formation of the interphase in PO-SWNTs nanocomposites is dominated by non-bonding contributions such as Van der Waals interactions, dipole–dipole (and dipole–dipole induced) interactions as well as molecular entanglements. Within the interphase, the nanofiller may capture atoms (such as C, O, H), groups of atoms (such as C–C, C–O, C–H, H–C–H), or even polymeric segments. Motions relevant to some of these bonds were noticed by Raman spectroscopy. Van der Waals interactions strongly dependent on the distance between the atoms (polymeric segments) and the nanofiller may explain such a capturing of atoms as the distance between these atoms and the nanofiller drops below a critical distance d*. These atoms remain captured if the chemical bond strength is balanced by the Van der Waals interactions.

Additional interactions and interlocking mechanisms may also contribute. The experimental data suggests that the interphase is dominated by entanglements, non-bonding interactions, and eventually C–H, C–O, H–C–H, and C–C interactions involving defective nanotubes (or nanotube edges) and the polymeric matrix. Raman spectroscopy revealed three candidates for such interactions (C–C, C–H, and H–C–H bonds) that may connect the nanofiller to the polymeric matrix.

The as-obtained fraction of the interphase is rather small pointing towards a very thin interphase. This is expected as the polymeric segments (monomer) consist of few atoms and no special method to increase the thickness of the interphase was used. Thus, covalent or stable chemical bonds between the nanofiller and the polymeric matrix have a very low probability.

AUTHOR CONTRIBUTIONS

Mircea Chipara: Conceptualization (equal); writing – review and editing (equal). **Dorina Chipara:** Project administration (equal); visualization (equal). **Karen Martirosyan:** Formal analysis (equal); supervision (equal). **Ananta Adhikari:** Methodology (equal); resources (equal). **Alexandro Trevino:** Data curation (equal); methodology (equal); software (equal).

ACKNOWLEDGMENTS

This work was supported by NSF grant DMR 2122178 (URGV-UMN PREM).

DATA AVAILABILITY STATEMENT

The data that support the findings of this study are available from the corresponding author upon reasonable request.

ORCID

Mircea Chipara https://orcid.org/0000-0003-3584-4863

REFERENCES

[1] L. Si, M. V. Massa, K. Dalnoki-Veress, H. R. Brown, R. A. L. Jones, *Phys. Rev. Lett.* **2005**, *94*, 1.
[2] B. O'Shaughnessy, *Phys. Rev. Lett.* **1987**, *59*, 2903.
[3] M. Bulacu, *Molecular Dynamics Studies of Entangled Polymer Chains*, Ph. D. Thesis, Rijks Universiteit, Groningen, Netherlands **2008**.
[4] S. El Fassi, M. Benhamou, M. Boughou, H. Kaidi, M. El Yaznasni, H. Ridouane, *Acta Phys. Polym. A.* **2010**, *118*, 606.
[5] Y. Li, J. Z. Xu, L. Zhu, G. J. Zhong, Z. M. Li, *J. Phys. Chem. B* **2012**, *116*, 14951.
[6] A. V. Sechkarev, N. I. Dvorovenko, *Soviet Phys. J.* **1969**, *9*, 1.
[7] A. Dondos, E. Pierri, E. Pierr, *Polym. Bull.* **1986**, *16*, 567.
[8] I. A. Tsebrenko, V. A. Pakharenko, *Fibre Chem.* **1999**, *31*, 197.
[9] H. Kang, X. Qian, L. Guan, M. Zhang, Q. Li, A. Wu, M. Dong, *Nanoscale Res. Lett.* **2018**, *13*, 5.
[10] H. Wang, *Science* **2009**, *323*, 757.
[11] M. B. Institut, *J. Polym. Sci. B Polym. Phys.* **2008**, *46*, 1556.
[12] S. Xu, P. A. O'Connell, G. B. McKenna, *J. Chem. Phys.* **2010**, *132*, 1.
[13] T. Sasaki, M. Misu, T. Shimada, M. Teramoto, *J. Polym. Sci. B Polym. Phys.* **2008**, *46*, 2116.
[14] S. Peter, H. Meyer, J. Baschnagel, *J. Polym. Sci. B Polym. Phys.* **2006**, *44*, 2951.
[15] P. G. De Gennes, *Eu. Phys. J. E* **2000**, *2*, 201.
[16] Y. T. Wang, T. C. Chang, Y. S. Hong, H. B. Chen, *Thermochim. Acta* **2003**, *397*, 219.
[17] J. S. João, A. A. Ribeiro, C. X. Cardoso, *Mater. Sci. Eng. B Solid State Mater. Adv. Technol.* **2007**, *136*, 123.
[18] E. C. Chen, T. M. Wu, *Polym. Degrad. Stab.* **2007**, *92*, 1009.

[19] X. Wu, J. Qiu, P. Liu, E. Sakai, *J. Polym. Res.* **2013**, *20*, 284.
[20] M. M. Hasan, Y. Zhou, S. Jeelani, *Mater. Lett.* **2007**, *61*, 1134.
[21] Y. Zou, Y. Feng, L. Wang, X. Liu, *Carbon N Y* **2004**, *42*, 271.
[22] M. Chipara, K. Lozano, A. Hernandez, M. Chipara, *Polym. Degrad. Stab.* **2008**, *93*, 871.
[23] S. Arepalli, P. Nikolaev, O. Gorelik, V. G. Hadjiev, W. Holmes, B. Files, L. Yowell, *Carbon N Y* **2004**, *42*, 1783.
[24] H. M. Duong, E. Einarsson, J. Okawa, R. Xiang, S. Maruyama, *Jpn. J. Appl. Phys.* **2008**, *47*, 1994.
[25] S. Arepalli, S. W. Freiman, S. Hooker, K. Migler, *Measurement Issues in Single-Wall Carbon Nanotubes*, National Institute of Standards and Technology, Gaithersburg, MD **2008**, p. 81.
[26] D. Bom, R. Andrews, D. Jacques, J. Anthony, B. Chen, M. S. Meier, J. P. Selegue, *Nano Lett.* **2002**, *2*, 615.
[27] C. Marazzato, Y. Peneva, E. Lefterova, S. Filippi, L. Minkova, *Polym. Test.* **2007**, *26*, 526.
[28] J. Heidarian, A. Hassan, *Asian J. Chem.* **2015**, *27*, 1235.
[29] P. Pereira, H. Gaspar, L. Fernandes, G. Bernardo, *Polym. Test.* **2015**, *47*, 130.
[30] X. Shi, B. Jiang, J. Wang, Y. Yang, *Carbon N Y* **2012**, *50*, 1005.
[31] V. Stefov, M. Najdoski, G. Bogoeva-Gaceva, A. Buzarovska, *Synth. Met.* **2014**, *197*, 159.
[32] A. C. Dillon, T. Gennett, P. A. Parilla, J. L. Alleman, K. M. Jones, M. J. Heben, *Evaluating the Purity of Single-Wall Nanotube Materials*, Materials Research Society Symposium–Proceedings, New York **2001**, p. 1. https://doi.org/10.1557/proc-633-a5.2
[33] J. Li, Y. Zhang, *Phys. E Low Dimen. Syst. Nanostruct.* **2005**, *28*, 309.
[34] J. H. Lehman, M. Terrones, E. Mansfield, K. E. Hurst, V. Meunier, *Carbon N Y* **2011**, *49*, 2581.
[35] W. Brostow, R. Chiu, I. M. Kalogeras, A. Vassilikou-Dova, *Mater. Lett.* **2008**, *62*, 3152.
[36] S. Espindola, B. Norder, S. J. Picken, *ACS Biomater. Sci. Eng.* **2023**, *24*, 1627.
[37] Z. M. Ao, Q. Jiang, *Langmuir* **2006**, *22*, 1241.
[38] M. I. Chipara, *Phys. B Condens. Matter.* **1997**, *234*, 263.
[39] S. Kawasaki, Y. Matsuoka, T. Yokomae, Y. Nojima, F. Okino, H. Touhara, H. Kataura, *Carbon N Y* **2005**, *43*, 37.
[40] A. Cao, C. Xu, J. Liang, D. Wu, B. Wei, *Chem. Phys. Lett.* **2001**, *344*, 13.
[41] D. M. Chipara, A. C. Chipara, M. Chipara, *Spectroscopy* **2011**, *26*, 2.
[42] Y. Park, K. P. S. S. Hembram, R. Yoo, B. Jang, W. Lee, S. G. Lee, J. G. Kim, Y. Il Kim, D. J. Moon, J. K. Lee, J. K. Lee, *J. Phys. Chem. C* **2019**, *123*, 14003.

How to cite this article: M. Chipara, D. Chipara, K. Martirosyan, A. Adhikari, A. Trevino, *J. Appl. Polym. Sci.* **2024**, *141*(4), e54850. https://doi.org/10.1002/app.54850